

## Nonlinear diffusion effects on biological population spatial patterns

Eduardo H. Colombo<sup>1</sup> and Celia Anteneodo<sup>1,2</sup><sup>1</sup>*Department of Physics, PUC-Rio, Rio de Janeiro, Brazil*<sup>2</sup>*National Institute of Science and Technology for Complex Systems, Rio de Janeiro, Brazil*

(Received 25 June 2012; published 27 September 2012)

Motivated by the observation that anomalous diffusion is a realistic feature in the dynamics of biological populations, we investigate its implications in a paradigmatic model for the evolution of a single species density  $u(x,t)$ . The standard model includes growth and competition in a logistic expression, and spreading is modeled through normal diffusion. Moreover, the competition term is nonlocal, which has been shown to give rise to spatial patterns. We generalize the diffusion term through the nonlinear form  $\partial_t u(x,t) = D \partial_{xx} u(x,t)^\nu$  (with  $D, \nu > 0$ ), encompassing the cases where the state-dependent diffusion coefficient either increases ( $\nu > 1$ ) or decreases ( $\nu < 1$ ) with the density, yielding subdiffusion or superdiffusion, respectively. By means of numerical simulations and analytical considerations, we display how that nonlinearity alters the phase diagram. The type of diffusion imposes critical values of the model parameters for the onset of patterns and strongly influences their shape, inducing fragmentation in the subdiffusive case. The detection of the main persistent mode allows analytical prediction of the critical thresholds.

DOI: [10.1103/PhysRevE.86.036215](https://doi.org/10.1103/PhysRevE.86.036215)

PACS number(s): 89.75.Kd, 89.75.Fb, 05.65.+b, 05.40.-a

### I. INTRODUCTION

Pattern formation in population dynamics has been studied both experimentally and theoretically. In experiments, the dynamics of insects and bacterial colonies, amongst others, have been observed [1–5]. From the theoretical viewpoint, mean-field descriptions render macroscopic or mesoscopic approximations to describe the behavior of such complex systems. To take into account spatial inhomogeneities, one may construct a partial differential equation that rules the temporal evolution of the population density  $u(\vec{x},t)$ , a function of the spatial position  $\vec{x}$  and time  $t$ . Within this family of models, a standard one was first introduced by Fisher [6]. It consists of a reaction-diffusion equation, taking into account growth and competition in the usual logistic form. Recently, a generalization of the Fisher equation (FE) was introduced [7–9], namely,

$$\frac{\partial}{\partial t} u(\vec{x},t) = D \nabla^2 u(\vec{x},t) + u(\vec{x},t)(a - bJ[u(\vec{x},t)]), \quad (1)$$

where  $D, a, b$  are positive parameters and  $J$  is a functional of the density embodying nonlocality:

$$J[u(\vec{x},t)] = \int_{\Omega} f(\vec{x},\vec{x}') u(\vec{x}',t) d\vec{x}'. \quad (2)$$

In the particular case  $f(\vec{x},\vec{x}') = \delta(\vec{x} - \vec{x}')$ , the original (local) FE is recovered. The introduction of the nonlocal form of the competition term is motivated by the consideration that products released in the environment by the individuals may either harm or support neighbors' growth. Interestingly, this nonlocal component was shown to give rise to the formation of steady spatial patterns [8]. Diverse variants have been studied before. As influence functions  $f(\vec{x},\vec{x}')$ , square and smooth forms have been considered [8,9]. Nonlocality in the reproduction rate [2], dimensionality [10], and fluctuation effects [11] have been investigated too. In all those cases, however, spatial spread was described by normal diffusion. Meanwhile, there are indications that the spreading of biological populations is

not due to purely random motion but influenced by the density, either to favor or to avoid crowding [12–14]. Hence dispersal is guided by a state-dependent diffusion coefficient rather than by a constant one.

An important class of generalized diffusion equations is constituted by the porous media equation  $\partial_t u = \partial_{xx} u^\nu$ , originally defined for  $\nu > 1$  [15]. Although it was later extended to real  $\nu > -1$  [16], here we will restrict our analysis to  $\nu > 0$ . Nonlinear diffusion is ruled by a state-dependent diffusion coefficient, proportional to  $u^{\nu-1}$ , hence embracing the cases where the coefficient either grows [17] or decreases [18] with the density  $u$ . The generalization of Arrhenius law [19], the performance of thermal ratchets [20], and other properties such as aging [21] that arise under this kind of diffusion have been studied before. Nonlinear diffusion equations in higher dimensions [22] or even with space-fractional derivatives [23] have been analytically solved. The nonlinearity leads to anomalous diffusion [16]: either superdiffusion for  $\nu < 1$  or subdiffusion for  $\nu > 1$ , recovering normal diffusion when  $\nu = 1$ . Microscopically, high density regions can slow down ( $\nu < 1$ ) or intensify ( $\nu > 1$ ) individual displacements, as a consequence of homophilic behaviors that rule the dynamics of self-diffusion favoring, or not, the mobility among other individuals. While  $\nu < 1$  reflects a reaction to sparseness (with high diffusion coefficients where the density is low), on the contrary,  $\nu > 1$  is associated with immobilization in poorly populated regions.

We will analyze the effects of nonlinear diffusion on pattern formation by considering the one-dimensional generalized FE with nonlocal competition

$$\frac{\partial}{\partial t} u(x,t) = D \frac{\partial^2}{\partial x^2} u^\nu(x,t) + u(x,t)(a - bJ[u(x,t)]). \quad (3)$$

Since alternative forms of the functional  $f(x,x')$  do not yield substantially different results [8], we will restrict our analysis to the case where  $f(x,x')$  is constant for  $x - w \leq x' \leq x + w$ ,

and zero otherwise, namely,  $f(x, x') = \frac{1}{2w} \Theta(w - |x - x'|)$ , where  $\Theta$  is the Heaviside step function.

## II. RESULTS

Numerical integration of Eq. (3) was performed by means of a standard forward-time centered-space scheme with integration time step  $dt \leq 10^{-3}$  and width of spatial grid cells  $dx \leq 0.1$ . We set periodic boundary conditions, with periodic domain size  $L = 100$ . As initial condition we considered small amplitude random perturbations either above the null state or around the nontrivial homogeneous solution. We also considered square pulses (with small random fluctuations) with zero values everywhere else.

Typical long-time patterns, robust under changes in the initial conditions here considered, are shown in Fig. 1. Notice that, while the number of peaks is not affected by changing  $\nu$ , the form of the patterns becomes substantially different. By increasing  $\nu$ , the width (inverse concavity) of the crests increases and the density at the valleys decreases, such that for  $\nu > 1$  disconnected regions can arise.

Figure 2 shows the time evolution for  $\nu = 4$ , starting with small random values of the density  $u(x, 0)$ . It rapidly increases for all  $x$  towards the level corresponding to the homogeneous solution,  $u_0 = a/b$  ( $t < 10$ ), while patterns develop. After  $t = 100$  no substantial changes are detected at the crests. Between successive crests, the density tends to zero (exponentially fast with time). This fragmentation or clusterization process [24] yields isolated population groups (clusters). Therefore fluxes between clusters are eliminated in the long-time limit. This

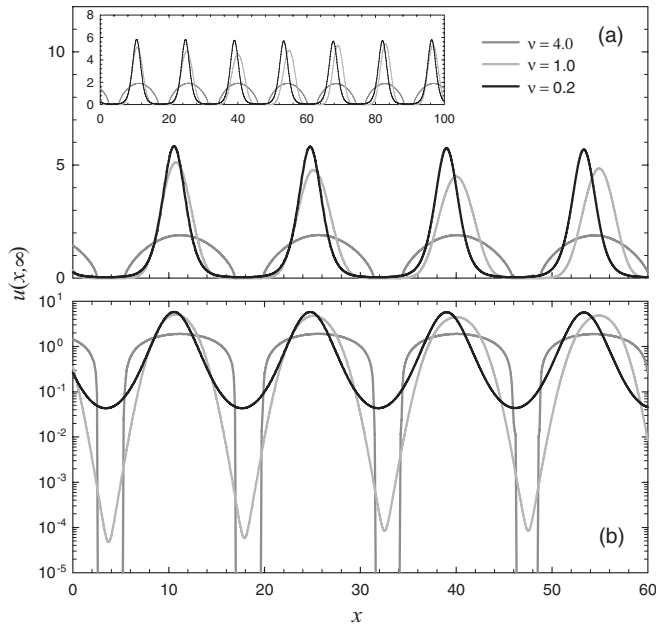


FIG. 1. Long-time patterns obtained from numerical integration of Eq. (3), with  $a = b = 1$ ,  $L = 100$ ,  $D = 0.1$ ,  $w = 10$ , and different values of  $\nu$  indicated on the figure, in (a) linear and (b) logarithmic scales. In the inset, the long-term profiles in the full grid are shown. The profiles are plotted for  $t = 200$ , but they remain unchanged after  $t \simeq 100$ .

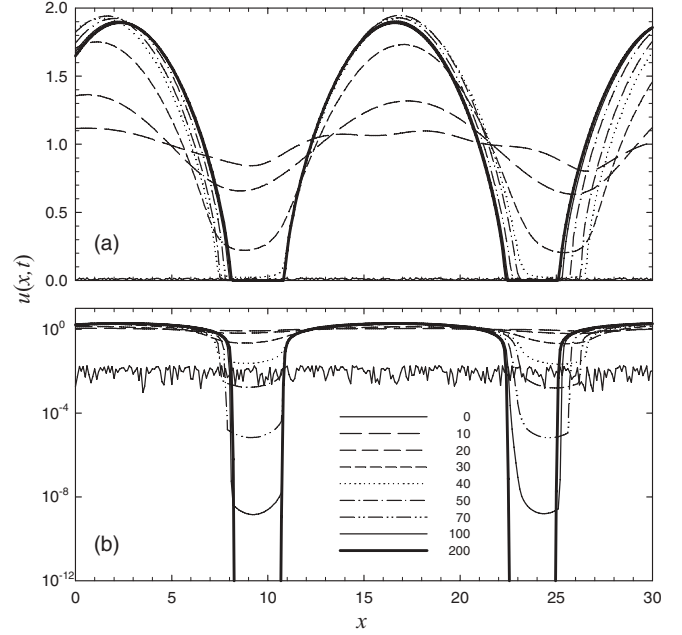


FIG. 2. Time evolution of the density profile obtained from numerical integration of Eq. (3) with  $a = b = 1$ ,  $L = 100$ ,  $D = 0.1$ ,  $w = 10$ , and  $\nu = 4$ , represented for different times  $t$  indicated on the figure, in (a) linear and (b) logarithmic scales. The thick line corresponds to  $t = 200$ .

phenomenon is crucial in connection with “epidemic” spreads within a population.

### A. Stability analysis

To determine the stability conditions we follow the standard procedure of considering a first-order perturbation around the homogeneous solution  $u_0 = a/b$ :

$$u(x, t) = u_0 + \epsilon \exp(ikx + \lambda_k t), \quad (4)$$

where  $\epsilon$  is the perturbation initial amplitude,  $k$  is the wave number, and  $\lambda_k$  is the exponential rate of temporal behavior. Substituting Eq. (4) into Eq. (3) gives the dispersion relation

$$\lambda_k = -\nu D u_0^{v-1} k^2 - a \frac{\sin(wk)}{wk}, \quad (5)$$

which generalizes the one obtained by Fuentes *et al.* [9]. Defining the nondimensional rate  $\Lambda_k \equiv \frac{\lambda_k}{a}$ , Eq. (5) can be rewritten in a single parameter form as

$$\Lambda_k = -\beta (wk)^2 - \frac{\sin(wk)}{wk}, \quad \text{with} \quad \beta \equiv \frac{\nu D u_0^{v-1}}{aw^2}. \quad (6)$$

Negative  $\Lambda_k$  means relaxation back to the uniform state. Figure 3 depicts the dispersion relation in a typical case where  $\Lambda_k$  can take positive values allowing instability growth.

Even if the analysis at short times does not guarantee the later evolution towards a stationary state, the mode with largest growth rate  $k^*$  (absolute maximum of the dispersion relation  $\Lambda_k$  vs  $k$ ) could play a crucial role. This mode will excite other wavelengths though the coupling nonlinear term; however, if they are damped,  $k^*$  will remain selected and its harmonics will shape the patterns. Substitution of the Fourier series expansion  $u(x, t) = \sum_{k=-\infty}^{\infty} c_k(t) \exp(ikx)$  into Eq. (3),

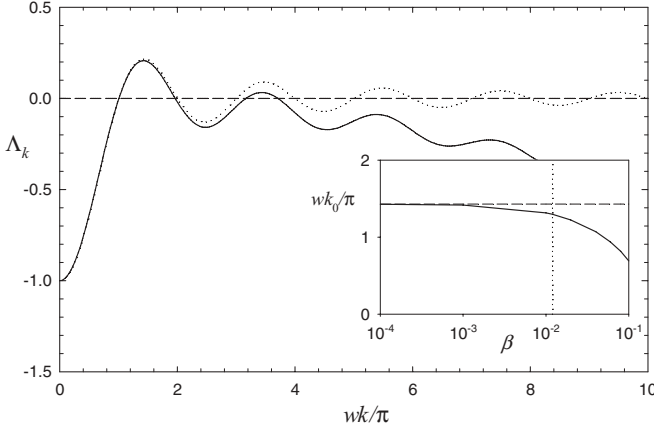


FIG. 3. Dispersion relation  $\Lambda_k = \lambda_k/a$  vs scaled  $k$  (solid line), for  $\beta = 5 \times 10^{-4}$ . The dotted line corresponds to the term  $-\sin(wk)/(wk)$  and the dashed line to the zero line, drawn for comparison. In the inset, we show the position of the first maximum  $k_0$  as a function of  $\beta \equiv vDu_0^{v-1}/(aw^2)$ . The vertical dotted line indicates the instability threshold.

when  $v = 1$ , leads to the following evolution equations for the Fourier coefficients  $c_k$  [9]:

$$\frac{dc_k}{dt} = -Dk^2c_k + ac_k - b \sum_m c_m \bar{c}_{k-m} \frac{\sin mw}{mw}. \quad (7)$$

These equations are highly coupled through the last nonlinear term. If  $v \neq 1$ , there will still be an additional nonlinearity in the first term of the right-hand side; anyway, let us consider the case where the first term is very small, allowing the existence of unstable modes. The amplitude of the mode corresponding to the uniform state,  $c_0$ , grows with rate  $a$  until stabilization, as observed in numerical simulations, e.g., in the example of Fig. 2 the level  $u_0 = a/b = 1$  is attained at times of order  $1/a$ . The mode with largest initial (positive) rate quickly develops and keeps dominating at intermediate timescales. Notice in Fig. 2 an almost perfect sinusoidal profile at time  $t \simeq 20$ . If a unique mode contributes to the sum in Eq. (7), it grows with the rate given by Eq. (5) until stabilization, while the remaining modes will be dumped. Actually a set of undamped harmonics, characteristic of each value of  $v$ , also persists to shape the profiles. Typical Fourier spectra for the long-term patterns are shown in Fig. 4. Although we do not have a rigorous mathematical proof, we will see that numerical results indicate that the dominant persistent mode, defining pattern wavelength, is the fastest growing one at short times.

$\Lambda_k$  possesses infinite local maxima located at  $k_n$ ,  $n = 0, 1, \dots$ . Since the absolute maximum is the first one, then  $k^* = k_0$  (see Fig. 3). In the inset of Fig. 3,  $k_0$  (numerically obtained) is plotted as a function of  $\beta$ . For sufficiently small  $\beta$ ,  $\Lambda_k$  is dominated by the last term in Eq. (6), yielding  $k_0 = \theta_0/w$  with  $\theta_0 \simeq 1.43\pi$ . Figure 4 shows that the dominant mode of long-time patterns is in good accord with  $k_0$ .

Perturbations to the homogeneous solution vanish if  $\Lambda_k < 0$ . Since  $\sin(wk)$  is bounded, then the instability condition  $\Lambda_k > 0$  implies

$$\beta < (wk)^{-3}. \quad (8)$$

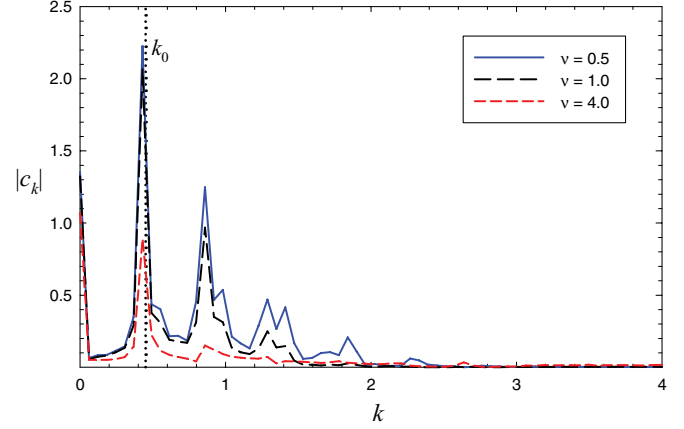


FIG. 4. (Color online) Fourier spectra for the long-time patterns shown in Fig. 1. The vertical dotted line indicates the position of the dominant mode  $k_0$ .

For the mode with largest growth, considering the approximation  $k_0 = \theta_0/w \simeq 1.43\pi/w$ , one has the instability condition

$$\beta \equiv \frac{vDu_0^{v-1}}{aw^2} < \theta_0^{-3} \simeq (1.43\pi)^{-3}. \quad (9)$$

This is equivalent to requiring the positivity of the first maximum. Notice in the inset of Fig. 3 that  $k_0 \simeq 1.43\pi/w$  remains a good approximation in the whole instability region, below the threshold (vertical dotted line in the inset). Beyond this point the maximum becomes negative, hence the homogeneous solution recovers its stability for any wavelength. Equation (9) defines the critical value  $\beta_c \equiv \theta_0^{-3}$  for the onset of patterns.

As intuitively expected, on the basis of the homogenizing role of diffusion, the inequality in Eq. (9) indicates that the diffusion constant cannot exceed a limiting value for the perturbation to depart from the homogeneous state. In accord with Eq. (9), in the limit  $D \rightarrow 0$ , patterns are also observed. Then, diffusion is not a necessary ingredient for the onset of patterns but has a role in pattern shaping. Figure 5(a) shows the density profiles that emerge for different values of  $D$  in the normal case  $v = 1$ . For  $D = 0$  patterns are noisy due to the lack of the smoothing effect of diffusion and the amplitude is less uniform but the wavelength  $\ell$  is well defined. Moreover, between bumps, the density tends to zero as in the subdiffusive case of Fig. 2. The width of the bump at zero height,  $2x_0$ , is also well defined. Beyond fluctuations, the results are robust, at least under the types of initial conditions analyzed. In the absence of diffusion, the steady state must verify  $u(x)[a - bJ(x)] = 0$ , then either  $u(x)$  vanishes or its integral within the interval  $(x - w, x + w)$  must adopt the constant value  $a/b$ . The former case requires that the null solution becomes stable in some regions. The latter requires that each cluster does not see the neighbors and any point in the cluster must be influenced by the full cluster. This means that  $2x_0 \leq w \leq \ell - 2x_0$ , which is verified in numerical experiments.

For  $D = 10^{-5}$ , patterns are still noisy at  $t = 100$ , but are expected to smooth out at much longer times. In this case also the density between crests goes to zero exponentially fast with time, as can be seen in Fig. 5(b). In the case of the figure, the

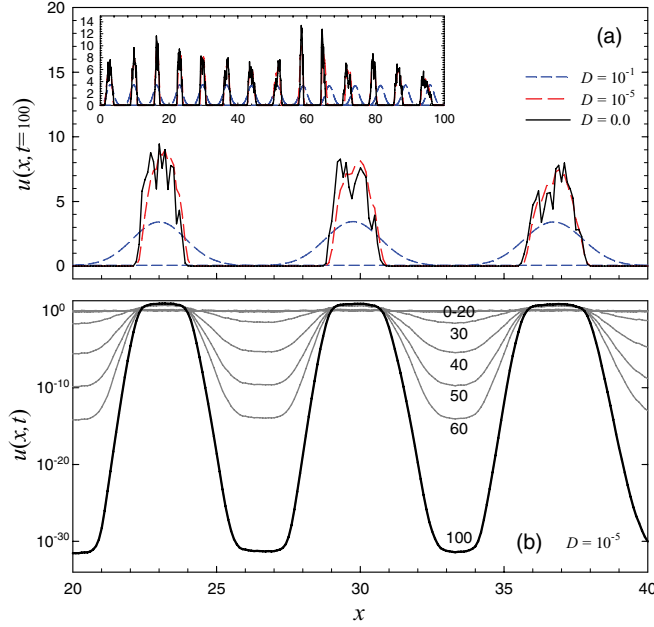


FIG. 5. (Color online) (a) Long-time patterns obtained from numerical integration of Eq. (3) up to time  $t = 100$ , with  $a = b = 1$ ,  $\nu = 1$ ,  $w = 5$ ,  $L = 100$ , and different values of  $D$  indicated on the figure. In the inset, the profiles in the full grid are shown. In (b) the time evolution for  $D = 10^{-5}$  is shown in logarithmic scale. Times are indicated in the figure.

clusterization occurs for  $D \lesssim 10^{-3}$ , while for larger values of  $D$  not only the crests but also the valleys stabilize in a finite value as time goes by. Then clusterization occurs for  $D$  below a threshold value only. Note the resemblance of the noisy profiles with those observed in experiments with bacteria [4]. But here clusters arise naturally, without imposing absorbing or zero flux boundaries.

If  $D \neq 0$ , Eq. (9) predicts the existence of a minimal value of the interaction range  $w$  required for pattern formation, with all other parameters kept fixed. This critical value depends on the kind of diffusion through the factors  $\nu$  and  $u_0^{\nu-1}$ . Note also that for  $\nu \neq 1$  there is an influence of  $u_0$  too, which is absent in the normal case ( $\nu = 1$ ).

According to the hypothesis that  $k_0$  is the characteristic wave number of the stationary pattern, and taking into account that boundary conditions are periodic (i.e., an integer number of wavelengths must accommodate to the size of the system  $L$ ), the number of maxima  $m$  is given (on average) by

$$m = \frac{k_0 L}{2\pi} = \frac{\theta_0}{2\pi} \frac{L}{w} \simeq 0.715 \frac{L}{w}. \quad (10)$$

Even in the cases when Eq. (10) gives an integer value, it is expected to furnish the number of peaks observed in the average. In practice, depending on the initial conditions, the crests come out and grow accommodating its number approximately to the rounded value of  $m$ . Fluctuations in the effective  $m$  are larger the larger  $m$  or the further is  $m$  from an integer value. For instance, in the example of Fig. 1, instead of seven, eight crests are observed in some realizations, being  $m \simeq 7.15$ .

These observations can be verified through numerical integration of the evolution equation. In Fig. 6, we show the

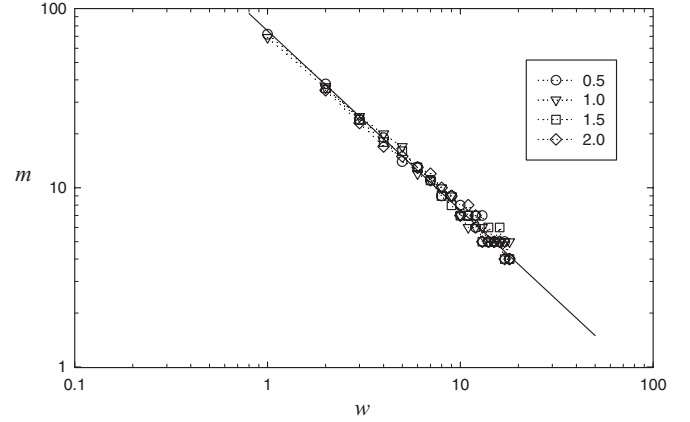


FIG. 6. Number of maxima  $m$  as a function of the nonlocality width  $w$ , for  $a = b = 1$ ,  $L = 100$ , and  $D = 0.01$ , and different values of  $\nu$  indicated in the figure. The solid line corresponds to the approximate theoretical relation (10) and the symbols to the outcomes of numerical simulations.

number of maxima  $m$  of the patterns as a function of  $w$  together with the theoretical prediction given by Eq. (10). An excellent agreement between theoretical and numerical outcomes can be observed. Then, in good approximation, the dominant wavelength only depends on the relation  $L/w$  independently of the remaining parameters. However, these parameters determine pattern upraise through the critical value of  $\beta$ , given by Eq. (9), and may also influence pattern shape. In particular, on average,  $m$  does not depend on  $\nu$ , as can be observed in the example of Fig. 1. The wave number is preserved in the limit  $D \rightarrow 0$ , even if in approaching this limit more and more modes become unstable (i.e., more local maxima of  $\Lambda_k$  become positive), but the global maximum remains approximately the same. Then, diffusion is not necessary for pattern formation, nor does it influence the characteristic wavelength.

Notice also that condition (9) indicates that, although approximately the same number of maxima is expected independently of  $\nu$ , there are critical thresholds  $\nu_c$  beyond which no patterns occur. This is illustrated in Fig. 7 for the case  $a = b = 1$ , for which  $\nu_c = w^2 / (D\theta_0^3)$ .

When diffusion is anomalous,  $u_0 = a/b$  is also determinant of pattern formation. How the phase diagram is altered by changes in  $u_0$  is illustrated in Fig. 8. The shadowed area represents the region where no patterns emerge when  $u_0 = 1$ . For other values of  $u_0$ , only the frontier is shown. For  $u_0 \geq 1$ , the critical curve increases monotonically with  $\nu$ , such that only small  $\nu$  (superdiffusion) allows pattern formation for a given interaction range  $w$ , when the remaining parameters are kept fixed. However, the monotonic behavior of the critical curve is broken when  $u_0 < 1$ . Thus, for low values of  $w$  there is also an upper critical value of  $\nu$  for the onset of patterns, but for large  $w$ , patterns occur for any  $\nu$ .

## B. Patterns shape

Although the characteristic mode does not depend on  $\nu$ , its amplitude does. This is shown in Fig. 9 where the amplitude



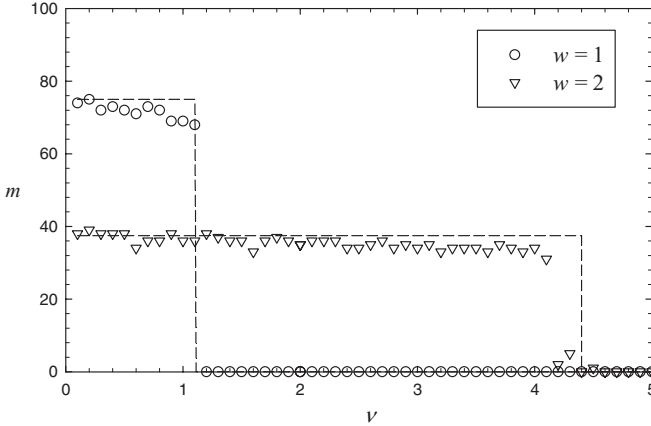


FIG. 7. Number of maxima  $m$  as a function of  $\nu$  for two different values of  $w$  indicated in the figure, with  $a = b = 1$ ,  $L = 100$ , and  $D = 0.01$ . Dashed lines correspond to the theoretical prediction given by Eq. (10), with the additional condition (9), defining a critical value  $\nu_c$  beyond which no patterns occur (we set  $m = 0$  in such case).

$\Delta u = u_{\max} - u_{\min}$  obtained from numerical simulations is represented as a function of  $w$  for different values of  $\nu$ .

For vanishing  $w$  we recover the local case  $f(x, x') = \delta(x - x')$  in which no patterns emerge, as supported by numerical simulations. In agreement with Eq. (9), there is a critical value  $w_c$ , at which the amplitude vanishes. Notice the abrupt decay of the amplitude at the critical value. This threshold was not detected in previous works dealing with normal diffusion possibly because of the range of parameters used. For instance, in Ref. [8],  $w_c/L$  would be of the order of  $10^{-3}$ . The critical value  $w_c$  decreases with  $\nu$ , indicating that a shorter influence range  $w$  is required when the dispersion passes from subdiffusive to superdiffusive. Then superdiffusion favors pattern formation and the amplitude of the patterns is larger. For  $w = L/2$  (or its multiples), the nonlocal term becomes  $J[u(x, t)] = J(t)$ , which follows the equation  $dJ/dt = (a - bJ)J$ . Then, in the long-time limit

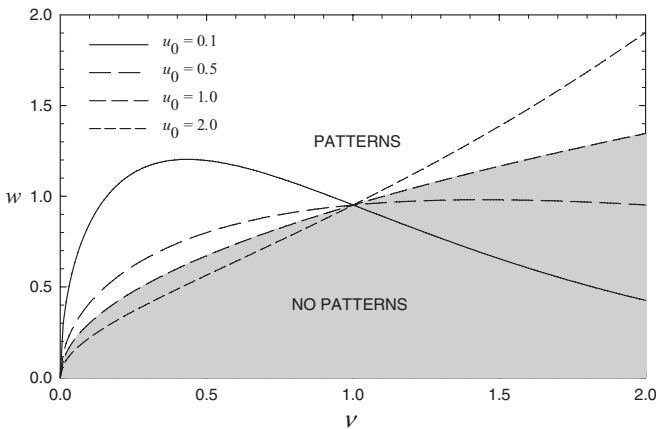


FIG. 8. Phase diagram of pattern formation in the  $\nu w$  plane, for  $u_0 = 1$ , following Eq. (9). Shaded is the region where no patterns arise. The lines show the frontier of the phase diagram for other values of  $u_0 = a/b$ . Patterns emerge for  $w > w_c$  (above the critical line). Parameter values are  $L = 100$ ,  $D = 0.01$ , and  $a = 1$ .

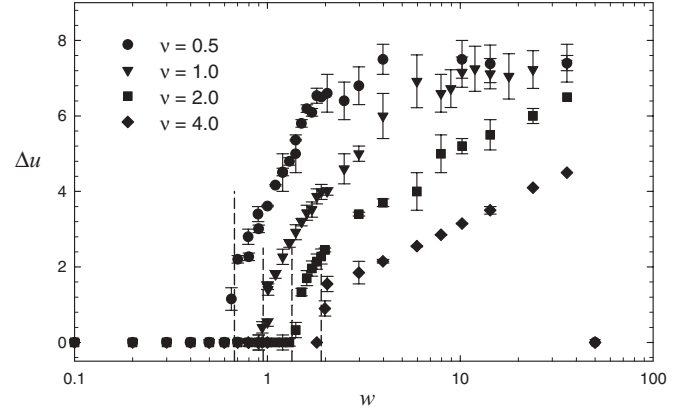


FIG. 9. Pattern amplitude  $\Delta u \equiv u_{\max} - u_{\min}$  as a function of the interaction width  $w$ , for  $a = b = 1$ ,  $L = 100$ ,  $D = 0.01$ , and different values of  $\nu$  indicated in the figure. The dotted lines are a guide to the eyes; the vertical ones indicate the critical value predicted by Eq. (9).

$J \rightarrow u_0$ , implying that the homogeneous state should also be attained in this extreme case.

Furthermore,  $\nu$  can have strong effects on patterns shape. As depicted in Fig. 1, subdiffusion ( $\nu > 1$ ) induces fragmentation (clusterization). Solutions that vanish outside a finite support are typical of nonlinear subdiffusion [12]. In the opposite case  $\nu < 1$  (superdiffusion), the effects are not so striking concerning pattern shape, for moderate values of the diffusion coefficient. The region between crests assumes larger values the smaller  $\nu$ . Fragmentation also emerges for any kind of diffusion when  $D$  is small enough (as discussed in connection to Fig. 5) or also if  $w$  becomes large enough (not shown). The shape of the clusters depends on  $\nu$ . Their amplitude decays and their width increases as  $\nu$  increases.

It is noteworthy that the distance between crests (wavelength),  $\ell = L/m \simeq 1.4w$ , is larger than the interaction range  $w$ ; however, if the cluster size  $2x_0(w)$  is large enough, there can be an influence of one cluster over the two neighboring ones. When clusters are disconnected,  $2x_0 \lesssim \ell - w = 0.4w$  means that one cluster does not influence the neighbors. Otherwise they do, even if disconnected.

### III. FINAL REMARKS

Nonlinear diffusion is expected in the spreading of biological populations rather than normal diffusion, hence motivating the introduction of a state-dependent diffusion coefficient, as in Eq. (3). We have shown how pattern formation is altered in the presence of anomalous diffusion. Moreover, in all cases, the initially fastest growing mode remains selected at longer times. This observation allows one to obtain theoretical predictions that we verified through numerical integration of the evolution equation.

Then, it is clear that diffusion is not a necessary ingredient for the onset of patterns, nor does it have an impact on the characteristic wavelength, which depends only on the interaction range  $w$ . Furthermore, diffusion imposes a critical threshold of the model parameters for pattern formation. The type of diffusion regime has an impact on patterns shape, even if the characteristic mode is kept unchanged. An important qualitative change in the shape of patterns occurs mainly for  $\nu > 1$ , in

which case fragmentation of the population is induced. This effect is also observed for very small diffusion constant  $D$  and/or large interaction width  $w$ . The occurrence of fragmentation may have important consequences in disease dissemination and other spreading processes triggered by contacts between individuals. Superdiffusion ( $\nu < 1$ ) facilitates pattern formation, which can occur even for shorter interaction width  $w$  and manifests larger amplitudes than in normal diffusion.

Beyond the initial motivation of introducing nonlinear diffusion to the nonlocal FE, we uncovered aspects that apply

also to the normal diffusion case previously studied. The identification of the main mode selected at long times allows one to perform analytical predictions, which may be extended to tackle other variants of the model.

#### ACKNOWLEDGMENTS

We are grateful to Welles A. M. Morgado for useful discussions. We acknowledge partial financial support from CNPq and Capes (Brazilian Government Agencies).

- 
- [1] T. E. Woolley, R. E. Baker, E. A. Gaffney, and P. K. Maini, *Phys. Rev. E* **84**, 046216 (2011).
- [2] J. A. R. da Cunha, A. L. A. Penna, and F. A. Oliveira, *Phys. Rev. E* **83**, 015201 (2011).
- [3] R. F. Costantino, R. A. Desharnais, J. M. Cushing, and B. Dennis, *Science* **275**, 389 (1997).
- [4] N. Perry, *J. R. Soc., Interface* **4**, 379 (2005).
- [5] L. Giuggioli and V. M. Kenkre, *Physica D* **183**, 245 (2003).
- [6] R. A. Fisher, *Ann. Eugen.* **7**, 355 (1937).
- [7] V. M. Kenkre and M. N. Kuperman, *Phys. Rev. E* **67**, 051921 (2003).
- [8] M. A. Fuentes, M. N. Kuperman, and V. M. Kenkre, *Phys. Rev. Lett.* **91**, 158104 (2003).
- [9] M. A. Fuentes, M. N. Kuperman, and V. M. Kenkre, *J. Phys. Chem. B* **108**, 10505 (2004).
- [10] E. Brigatti, M. Núñez-López, and M. Oliva, *Eur. Phys. J. B* **81**, 321 (2011).
- [11] E. Brigatti, V. Schwämmle, and M. A. Neto, *Phys. Rev. E* **77**, 021914 (2008).
- [12] J. D. Murray, *Mathematical Biology: I. An Introduction*, Interdisciplinary Applied Mathematics, Vol. 17 (Springer, New York, 2002).
- [13] M. E. Gurtin and R. C. MacCamy, *Math. Biosci.* **33**, 35 (1977).
- [14] S. E. Mangioni, *Physica A* **391**, 113 (2012).
- [15] M. Muskat, *The Flow of Homogeneous Fluids through Porous Media* (McGraw-Hill, New York, 1937); L. A. Peletier, in *Applications of Nonlinear Analysis in the Physical Sciences*, edited by H. Amann, N. Bazley, and K. Kirchgassner (Pitman, London, 1981).
- [16] C. Tsallis and D. J. Bukman, *Phys. Rev. E* **54**, R2197 (1996).
- [17] J. Buckmaster, *J. Fluid Mech.* **81**, 735 (1977); E. W. Larsen and G. C. Pomraning, *SIAM J. Appl. Math.* **39**, 201 (1980); W. L. Kath, *Physica D* **12**, 375 (1984); H. Spohn, *J. Phys. I* **3**, 69 (1993).
- [18] P. Rosenau, *Phys. Rev. Lett.* **74**, 1056 (1995); A. Compte, D. Jou, and Y. Katayama, *J. Phys. A* **30**, 1023 (1997); L. Borland, *Phys. Rev. Lett.* **89**, 098701 (2002).
- [19] E. K. Lenzi, C. Anteneodo, and L. Borland, *Phys. Rev. E* **63**, 051109 (2001).
- [20] C. Anteneodo, *Phys. Rev. E* **76**, 021102 (2007).
- [21] D. A. Stariolo, *Phys. Rev. E* **55**, 4806 (1997); L. Borland, *ibid.* **57**, 6634 (1998).
- [22] L. C. Malacarne, R. S. Mendes, I. T. Pedron, and E. K. Lenzi, *Phys. Rev. E* **65**, 052101 (2002).
- [23] E. K. Lenzi, G. A. Mendes, R. S. Mendes, L. R. da Silva, and L. S. Lucena, *Phys. Rev. E* **67**, 051109 (2003).
- [24] E. Hernández-García, C. López, S. Pigolotti, and K. H. Andersen, *Philos. Trans. R. Soc. London, Ser. A* **367**, 3183 (2009).